JOURNAL OF AIRCRAFT
Vol. 40, No. 5, September–October 2003

Robust Aeroservoelastic Design with Structural Variations and Modeling Uncertainties

Moti Karpel,* Boris Moulin,† and Moshe Idan‡
Technion—Israel Institute of Technology, 32000 Haifa, Israel

An aeroservoelastic analysis procedure has been integrated with structural optimization and robust-control design tools. The multidisciplinary analysis and design process can address structural constraints, performance, and robust aeroservoelastic stability requirements simultaneously. The design process is expanded to account for structural variations and modeling uncertainties utilizing a reduced-order state-space model of the aeroelastic plant that is advantageous for efficient low-order controller design. Reduced-order modeling introduces unstructured modeling errors. Structural mass variations, such as those associated with a wide range of changeable external stores of a fighter aircraft, are also interpreted as model uncertainties. The models are expressed in a form compatible with standard robust control design procedures such as the μ synthesis and analysis technique incorporated in this study. The robust control system can then be included in an optimization process where more elaborate aeroelastic models are used for tuning selected structural variables and control gains for minimizing specific design objectives under stability, performance, and structural integrity requirements. To provide enhanced physical insight, the μ analysis procedure is supplemented by a technique for computing stability boundaries in multidimensional parametric uncertainty spaces that is based on the classical single-input/single-output gain-margin approach. The integrated design procedure is demonstrated with a realistic model of a fighter aircraft with four wing control surfaces and a wing-tip missile with variable inertial properties.

Introduction

AEROSERVOELASTICITY (ASE) deals with the interaction of aircraft structural, aerodynamic, and control systems. The interaction affects the aircraft performance, static and dynamic stability characteristics, structural integrity, handling qualities, development risks, and growth potential. The increasing demand for high-performance airplanes at affordable cost motivated the development of automated analysis and design schemes that can deal with all of the aeroservoelastic design requirements in an integrated manner.[1,2] The main aeroservoelastic issues considered in these software tools are static and dynamic design loads, associated stress and strain levels, aerodynamic stability derivatives, vibration levels, aeroelastic stability (divergence and flutter), control stability robustness, and continuous gust response.

Classical frequency-domain flutter analysis methods are based on modal representation of the structure and the associated transcendental unsteady aerodynamic generalized force coefficient matrices calculated for selected frequency values. Some control system effects can be accommodated by the frequency-domain approach, but the application of modern control design techniques requires the aeroservoelastic equations of motion to be cast in a first-order, time-domain (state-space) form. This representation requires the aerodynamic matrices to be approximated by rational functions in the complex Laplace domain. The minimum-state method[3,4] provides rational approximation expressions and yields state-space aeroelastic models with a minimal number of aerodynamic lag states per desired accuracy. These aeroelastic state-space models can be augmented by a control system model for aeroservoelastic studies with flutter, control stability margins, dynamic response, and continuous gust considerations.[2]

The formulation of Ref. 2 was utilized in an ASE software module that was designed to interconnect with other software packages for multidisciplinary design schemes.[5] The interconnections between the ASE module and other structural and control design tools are shown in Fig. 1. The ASE module reads the modal database generated by a standard finite element code and constructs the open-loop aeroelastic equations of motion in a linear state-space form. The other functions executed by the ASE module depend on the user-defined mission. The options include data generation for controller design using an external control synthesis tool, ASE analysis, sensitivity analysis, and data export for structural optimization. The ASE module was integrated in the ASTROS[6] structural optimization system and was included in the ZAERO aeroelastic code.[7]

The data exported by the ASE module for control synthesis may include full- or reduced-order aeroelastic state-space model matrices, their variations or sensitivities with respect to structural uncertainties, and ASE-related design constraints. When ASE analysis is requested, the aeroelastic state-space equations are augmented in the ASE module to include the control system. A general and flexible control system architecture is implemented in the ASE module[5] that is able to model any linear multi-input/multi-output (MIMO) controller. The module can be used to calculate open- and closed-loop flutter parameters and control margins associated with the user-defined control architecture and continuous gust response in statistical terms. These parameters and their analytical derivatives with respect to the design variables[2] can then be used by the structural optimization code as design constraints and sensitivities. In addition to structural design parameters, the design variables may include the control system parameters defined as variable gains in the controller formulation, as discussed and demonstrated in the numerical examples in Refs. 5 and 8.

Aeroservoelastic interaction affects almost all of the structural and control design constraints. However, it is not necessary to include all of the constraints in the two design schemes. Stress alleviation requirements, for example, can be represented in the control design by limiting the wing-root bending moments in gust response or static maneuvers. Maneuvering performance and control authority requirements, on the other hand, can be represented in the structural design by assigning aeroelastic effectiveness constraints, as done in

Received 1 August 2001; revision received 18 November 2002; accepted for publication 25 November 2002.

*Professor, Faculty of Aerospace Engineering. Associate Fellow AIAA.
†Senior Researcher, Faculty of Aerospace Engineering. Member AIAA.
‡Senior Lecturer, Faculty of Aerospace Engineering. Associate Fellow AIAA.

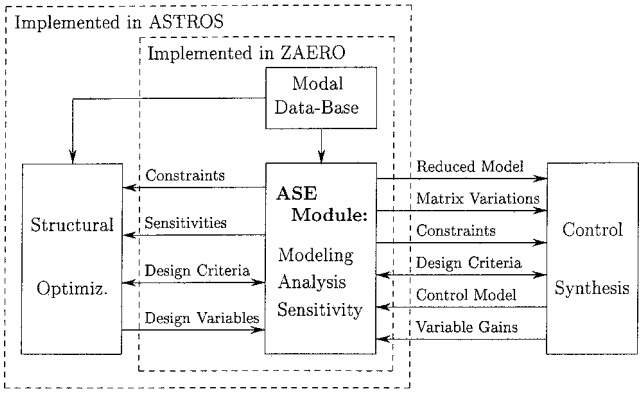

Fig. 1 Aeroservoelastic interconnections.

Ref. 5. Highly coupled issues such as flutter should be addressed in both schemes.

The new ASE procedures provide explicit expressions for all of the aeroservoelastic stability, response, and performance design constraints that can be adequately treated by linear models and their sensitivities to structural variables and control gains.[2] Because it is based on efficient reduced-size state-space models, the new ASE module is instrumental in robust-design procedures that require numerous repeated analyses with various design parameters and/or efficient perturbation models. A very promising approach within the ASE process is the application of new robust-control synthesis and analysis techniques, such as the structured singular value μ analysis and synthesis methods available as commercial software.[9] The fundamentals of robust ASE stability analysis are discussed in Ref. 10.

The study presented in this paper extends previous tools and methods derived to address emerging challenges of robust-aeroservoelastic-design methodologies and software modules in realistic design processes that involve structural uncertainties and robust-control requirements with strong aeroservoelastic coupling effects. It extends the procedures described in Ref. 5 that dealt mainly with the process of exporting plant models from the structural optimization process (using ASTROS) for classical design of low-order control system (using MATLAB®) and then importing the control model for final tuning of the structural and control variables. This line of research was further elaborated in Ref. 8, which focused on robust-MIMO aeroservoelastic-control design with structural uncertainties and performance requirements, using the μ synthesis and analysis approach, and the tradeoff between structural weight and control robustness. The current study expands the previous ones in the following directions: 1) Structured singular value analysis and design techniques are supplemented by a numerically robust procedure for direct computation of multidimensional stability boundaries, useful in guiding the multidisciplinary design process. 2) Structural variations are introduced as model perturbations in conjunction with state residualization to reduce the size of the control-design model. 3) The uncertainties introduced by the state residualization are included in the control design process, together with structural variations and performance requirements. 4) The design process is completed by a final tuning of selected structural and control variables using ASTROS. These theoretical results and numerical applications are described herein.

Aeroelastic Model

State-Space Equations of Motion

The ASE formulation in this paper follows the state-space formulation of Refs. 2, 5, and 8. The time-domain ASE models for stability and response analysis are constructed from the separate models of the aeroelastic plant and the control system expressed in a state-space form. The control system includes the control surfaces driven by actuators, sensors related to the structural degrees of freedom, and a linear MIMO control law that relates the actuator inputs to the sensor signals.

The formulation of the aeroelastic equations of motion in a state-space form is based both on expressing the structural displacement vector as a linear combination of a low-frequency set of normal modes and on expressing the generalized aerodynamic force coefficient matrices as rational functions of the Laplace variable (see Ref. 4). The open-loop ASE model is a result of the augmentation of the aeroelastic model and the state-space realization of the actuators, which leads to the plant equations

$$\{\dot{x}_p\} = [A_p]\{x_p\} + [B_p]\{u_p\} \tag{1a}$$

$$\{y_p\} = [C_p]\{x_p\} \tag{1b}$$

where $\{u_p\}$ is the vector of actuator inputs and $\{y_p\}$ is the vector of sensor signals. The vector of the plant states $\{x_p\}$ includes the vectors of n_h generalized displacements $\{\xi\}$ and n_h generalized velocities $\{\dot{\xi}\}$, n_a aerodynamic lag states $\{x_a\}$, and $3n_c$ actuator states $\{x_{ac}\}$ that comprise the displacements $\{\delta_c\}$, velocities $\{\dot{\delta}_c\}$, and accelerations $\{\ddot{\delta}_c\}$ of n_c control surfaces. Third-order actuator dynamics is assumed. Higher-order actuator dynamics and the sensor dynamics can be included as parts of the control system.

Equations (1) can be expressed explicitly according to the components $\{\xi\}$, $\{\dot{\xi}\}$, and $\{x_{ns}\}$ of the state vector $\{x_p\}$ as[8]

$$\begin{bmatrix} [I] & 0 & 0 \\ 0 & [\bar{M}_{hh}] & 0 \\ 0 & 0 & [I] \end{bmatrix} \begin{Bmatrix} \dot{\xi} \\ \ddot{\xi} \\ \dot{x}_{ns} \end{Bmatrix} = \begin{bmatrix} 0 & [I] & 0 \\ A_{21} & A_{22} & A_{23} \\ 0 & A_{32} & A_{33} \end{bmatrix} \begin{Bmatrix} \xi \\ \dot{\xi} \\ x_{ns} \end{Bmatrix} + \begin{bmatrix} 0 \\ 0 \\ B_{ns} \end{bmatrix} \{u_p\} \tag{2a}$$

$$\{y_p\} = [C_1 \quad C_2 \quad C_3] \begin{Bmatrix} \xi \\ \dot{\xi} \\ x_{ns} \end{Bmatrix} \tag{2b}$$

where $\{x_{ns}\}$ includes the nonstructural states $\{x_a\}$ and $\{x_{ac}\}$. The generalized mass matrix on the left-hand side of Eq. (2a) is

$$[\bar{M}_{hh}] = [M_{hh}] + (qb^2/V^2)\left[A_{hh_2}\right] \tag{3}$$

where $[M_{hh}]$ is the structural generalized mass matrix, q is the dynamic pressure, V is the true air speed, b is the reference semicord, and $[A_{hh_2}]$ is the apparent mass term of the aerodynamic approximation expression. The $[A_{ij}]$ and $[C_i]$ matrices in Eqs. (2) are functions of the structure modal properties and the other aerodynamic approximation terms, as detailed in Ref. 8.

Model Size Reduction

For efficient synthesis and analysis of control systems for the aeroservoelastic plant, reduced-order ASE models are highly desirable. It is especially important when modern multivariable robust-control design techniques are employed where the resulting order of the dynamic controller is usually higher than the order of the ASE plant. Hence, using reduced-order ASE models will generally result in lower-order controllers and may contribute to simplified controller synthesis and analysis procedures, in particular when iterative control design techniques such as μ synthesis are applied.

Model-order reduction is achieved by eliminating structural states that have a negligible effect on the model dynamics. Model-order reduction techniques based on residualization of the structural states are discussed in Ref. 11. The static residualization technique is applied in the current work to the aeroelastic system equations of motion before engaging in the controller design.

Model reduction starts by partitioning the structural states into two sets: the retained states $\{x_r\}$ that contain the $\{\xi_r\}$, $\{\dot{\xi}_r\}$, $\{x_a\}$, and $\{x_{ac}\}$ substate vectors and the eliminated states $\{x_e\}$ that contain $\{\xi_e\}$ and $\{\dot{\xi}_e\}$. The plant Eqs. (2) are restated as

$$\begin{bmatrix} Z_{rr} & Z_{re} \\ Z_{er} & Z_{ee} \end{bmatrix} \begin{Bmatrix} \dot{x}_r \\ \dot{x}_e \end{Bmatrix} = \begin{bmatrix} A_{rr} & A_{re} \\ A_{er} & A_{ee} \end{bmatrix} \begin{Bmatrix} x_r \\ x_e \end{Bmatrix} + \begin{bmatrix} B_r \\ 0 \end{bmatrix} \{u\} \tag{4a}$$

$$\{y\} = [C_r \quad C_e]\begin{Bmatrix} x_r \\ x_e \end{Bmatrix} \tag{4b}$$

The static residualization assumptions are that only the effects of the $\{\xi_e\}$ states in $\{x_e\}$ are important whereas the effects of $\{\dot{\xi}_e\}$ and $\{\ddot{\xi}_e\}$ are negligible. With these assumptions, the residualized model becomes

$$[\tilde{Z}]\{\dot{x}_r\} = [\tilde{A}]\{x_r\} + [\tilde{B}]\{u\} \tag{5a}$$

$$\{y\} = [\tilde{C}]\{x_r\} \tag{5b}$$

where

$$[\tilde{Z}] = \begin{bmatrix} [I] & 0 & 0 \\ 0 & [\tilde{M}^*_{rr}] & 0 \\ 0 & 0 & [I] \end{bmatrix} \tag{6a}$$

$$[\tilde{A}] = \begin{bmatrix} 0 & [I] & 0 \\ A^*_{21} & A^*_{22} & A^*_{23} \\ 0 & A_{32} & A_{33} \end{bmatrix} \tag{6b}$$

$$[\tilde{C}] = \begin{bmatrix} C^*_1 & C^*_2 & C^*_3 \end{bmatrix} \tag{6c}$$

and

$$\left[\tilde{M}^*_{rr}\right] = [\bar{M}_{rr}] - [A_{21,re}]\left[A^{-1}_{21,ee}\right][\bar{M}_{er}] \tag{7a}$$

$$\begin{bmatrix} A^*_{21} & A^*_{22} & A^*_{23} \end{bmatrix} = [A_{21,rr} \quad A_{22,rr} \quad A_{23,r}] - \left[A^{-1}_{21,ee}\right][A_{21,er} \quad A_{22,er} \quad A_{23,e}] \tag{7b}$$

$$\begin{bmatrix} C^*_1 & C^*_2 & C^*_3 \end{bmatrix} = [C_{1,r} \quad C_{2,r} \quad C_3] - [C_{1,e}]\left[A^{-1}_{21,ee}\right][A_{21,er} \quad A_{22,er} \quad A_{23,e}] + [C_{1,e}]\left[A^{-1}_{21,ee}\right]\begin{bmatrix} 0 & [\bar{M}_{er}]\left[\bar{M}^*_{rr}\right]^{-1} & 0 \end{bmatrix}[\tilde{A}] \tag{7c}$$

Uncertainty Models

Parameter Uncertainty

Modeling parametric variations or uncertainties of the ASE system is based on its sensitivity data and linear fractional transformation (LFT) tools.[12–14] The procedure presented in Ref. 8 can handle a variety of model uncertainties including variations in the stiffness and inertial properties, uncertainties in the aerodynamic data, and more. As an example, Moulin et al.[8] presented the modeling procedures to address variations in the total mass, moments of inertia, and center of gravity location of lumped inertia elements. LFT tools were used to represent these system variations as structured uncertainties. The uncertainty block introduced additional feedback paths in the ASE plant model that was based on 20 structural modes, namely, 40 structural states. In the present study, this technique is further expanded to facilitate state residualization that yields a significant reduction in the number of structural states.

With the fixed-basis modal approach, where the baseline vibration modes are used as a fixed set of generalized coordinates, inertial changes are reflected in the model through the perturbation $[\Delta M_{hh}]$ of the inertial matrix of Eq. (3) from its nominal value. The LFT expressions developed in Ref. 8 are applicable to the residualized system as well, with some modifications, which are given in this section.

The first step in modeling the inertial uncertainties for the residualized model of Eqs. (5) and (6) is to express the deviation of $[\tilde{M}^*_{rr}]$ in Eq. (7a) from its nominal values using the LFT structure. The perturbed matrix $[\tilde{M}^*_{rr}]$ for a linear uncertainty in the mass or the moment of inertia of the lumped structural elements can be expressed as

$$\left[\tilde{M}^*_{rr}\right] = \left[\bar{M}^*_{rr}\right] + \left[DM^*_{rr}\right]\delta \tag{8}$$

where $\delta \in [-1, 1]$ is the normalized uncertainty and

$$\left[DM^*_{rr}\right] = \left([\phi_{gr}]^T - [A_{21,re}]\left[A^{-1}_{21,ee}\right][\phi_{ge}]^T\right)\frac{\partial[M_{gg}]}{\partial m}[\phi_{gr}]k\bar{m} \tag{9}$$

where $[\phi_{gr}]$ and $[\phi_{ge}]$ are the retained and the eliminated normal modes, respectively, $[M_{gg}]$ is the global finite element mass matrix, $\bar{m}$ is a reference mass (or moment of inertia) value associated with the perturbed part of the structure, and k is its maximal relative perturbation, that is, $-k\bar{m} \le \Delta m \le k\bar{m}$. Static aeroelastic stability of the system guarantees $[A_{21,ee}]$ is invertible.

The dependence of the modal mass matrix on variations or uncertainty in the centers of gravity of the lumped mass elements is quadratic:

$$\left[\tilde{M}^*_{rr}\right] = \left[\bar{M}^*_{rr}\right] + \left[DM^{(1)^*}_{rr}\right]\delta + \left[DM^{(2)^*}_{rr}\right]\delta^2 \tag{10}$$

where $[DM^{(i)^*}_{rr}]$ are

$$\left[DM^{(i)^*_{rr}}\right] = \left[DM^{(i)}_{rr}\right] - [A_{21,re}]\left[A^{-1}_{21,ee}\right]\left[DM^{(i)}_{er}\right] \tag{11}$$

The sensitivities $[DM^{(i)}_{rr}]$ and $[DM^{(i)}_{er}]$ are defined in Ref. 8 according to the center of gravity offsets.

Equations (8) and (10) can be cast in a lower LFT form

$$\left[\tilde{M}^*_{rr}\right] = \mathcal{F}_\ell(\mathcal{M}, \Delta) = \mathcal{M}_{11} + \mathcal{M}_{12}\Delta(I - \mathcal{M}_{22}\Delta)^{-1}\mathcal{M}_{21} \tag{12}$$

where, for the linear dependence [Eq. (8)],

$$\mathcal{M} = \begin{bmatrix} \bar{M}^*_{rr} & DM^*_{rr} \\ I_r & 0 \end{bmatrix}, \qquad \Delta = [I_r]\delta \tag{13}$$

and for the quadratic dependence [Eq. (10)],

$$\mathcal{M}_{11} = \left[\bar{M}^*_{rr}\right], \qquad \mathcal{M}_{12} = \begin{bmatrix} DM^{(1)^*} & DM^{(2)^*} \end{bmatrix}$$

$$\mathcal{M}_{21} = \begin{bmatrix} I_r \\ 0 \end{bmatrix}, \qquad \mathcal{M}_{22} = \begin{bmatrix} 0 & 0 \\ I_r & 0 \end{bmatrix}, \qquad \Delta = [I_{2r}]\delta \tag{14}$$

For any number of parametric uncertainties in the ASE system, the perturbed matrix $[\tilde{M}^*_{rr}]$ is constructed as a sum of LFTs that can also be cast as an LFT. When the methodology developed in Ref. 8 is used, the equation of motion for the residualized perturbed plant can be obtained. The expressions for the residualized model are similar to those of the full-size one, except that the output equation becomes more complicated due to the influence of the inertia of the eliminated modes on the remaining ones. Full details of this model derivation can be found in Ref. 15. The resulting model of the uncertain residualized ASE plant is given by

$$\{\dot{x}_r\} = [A_r]\{x_r\} + [\tilde{B}_1]\{u_\delta\} + [B_r]\{u_p\} \tag{15a}$$

$$\{y_\delta\} = [\tilde{C}_1]\{x_r\} + [\tilde{D}_{11}]\{u_\delta\} \tag{15b}$$

$$\{y_r\} = [\tilde{C}]\{x_r\} + [\tilde{D}_{21}]\{u_\delta\} \tag{15c}$$

where $[A_r] = [\tilde{Z}]^{-1}[\tilde{A}]$ and $[B_r] = [\tilde{Z}]^{-1}[\tilde{B}]$.

In these equations, the system uncertainty is expressed by connecting the augmented inputs $\{u_\delta\}$ to the augmented outputs $\{y_\delta\}$ through the overall uncertainty block Δ that combines all of the possible physical variations and model uncertainties. In the nominal design case, the augmented inputs and outputs are zero. When $[\tilde{B}_1] = 0$ and $[\tilde{D}_{21}] = 0$ are set, Eqs. (15a) and (15c) revert back to the reduced-order ASE model of Eqs. (5).

As discussed in Ref. 15, the dependence of $[C^*_3]$ in Eq. (6c) on the modal mass matrix [see Eq. (7c)] increases the dimension of the uncertainty block four times. For acceleration measurements, the uncertainty model is even more complex. Therefore, one could consider ignoring the third term of the last row of Eq. (7c) to simplify the modeling of the uncertain system and the subsequent design. The implications of this simplification on the system robustness are typically negligible, as implied by the good results obtained in the subsequent numerical example.

Unmodeled Dynamics

The residualized ASE model used in control design is instrumental in constructing a low-order controller and is central in simplifying the design process. However, the residualization process may introduce dynamic differences between the full- and reduced-order ASE models that may cause unfavorable interaction between the resulting control system and the unmodeled high-frequency structural dynamics.

The control system designed using the residualized model is tested using the full-state ASE equations that best approximate the actual real-world operation mode. In most of the cases, the frequency content of the residualization errors are beyond the closed-loop bandwidth of the controlled ASE plant, leading to similar responses of the reduced- and full-order closed-loop systems. However, in some cases, the difference between the residualized and full-order systems is significant enough to cause degraded performance of the full closed-loop system and even instability. That spillover-type behavior is caused by the excitation of the neglected, mostly high-frequency, modes of the full-order model, not accounted for in the design using the reduced-order system.

To address this phenomenon, it is proposed to incorporate high-frequency uncertainty components in the reduced-order model. The goal of introducing these unstructured, frequency-dependent uncertainties is to capture the dynamic characteristics of model reduction errors by using low-order rational transfer matrices. Low-order uncertainty models are desirable here to ensure that the overall residualized system with uncertainties is still of a lower order than the full-order system, making the residualization process beneficial. The unstructured uncertainties can be constructed by fitting the residualization error with rational transfer matrices, using, for example, standard least-squares techniques.[16] The robust controllers designed with these uncertainties will account for the residualization errors, ultimately avoiding the excitation of the related high-frequency modes of the full-order system.

Stability Boundaries of Uncertain Systems

The aeroservoelastic stability boundaries are usually defined by the flight-envelope points (velocity and altitude) at which the system becomes unstable. When some structural, aerodynamic, or control parameters are uncertain, stability boundaries can be defined for a given flight condition within the flight envelope by multidimensional surfaces of the uncertain variables on which the system is neutrally stable. Even though robustness analysis and design can be performed without actually finding these stability boundaries, they are often desired to gain physical understanding and define limits for design tasks in the various disciplines.

The uncertainty models of the preceding sections can be used to find the stability boundaries of either the open-loop aeroelastic system of Eqs. (15) or the closed-loop aeroservoelastic system obtained after the control system augmentation[8,15] when both systems include the uncertainty-related inputs $\{u_\delta\}$ and outputs $\{y_\delta\}$. Nominal open-loop stability is determined by the eigenvalues of the matrix $[A_r]$ in Eq. (15a). To determine the open-loop stability of a perturbed system, the uncertainty-related input to output loops in Eqs. (15) must be closed with a particular uncertainty block $[\Delta]$, and the eigenvalues of the resulting perturbed system matrix

$$\left[A_r^{\text{pert}}\right] = [A_r] + [\tilde{B}_1][\Delta]([I] - [\tilde{D}_{11}][\Delta])^{-1}[\tilde{C}_1] \qquad (16)$$

must be computed.

Closed-loop stability can be determined from the open-loop nominal or perturbed system models using either classical single-input/single-output (SISO) or modern MIMO techniques. For this analysis, the appropriate aeroelastic model is augmented with a linear dynamic MIMO controller. This controller is structured according to the general architecture of Ref. 5 and comprises fixed, possibly dynamic components and variable gains. These variable gains are used in the stability margin evaluations and are usually subject to multidisciplinary optimization.

The classical closed-loop stability analysis is based on SISO gain- and phase-margin evaluation. In its standard form, the SISO stability margins determine the allowable complex perturbations in the gains of a static controller $\{u\} = [G]\{y\}$. In the ASE context, the matrix $[G]$ will include only the variable controller gains. Evaluation of the SISO stability margins for the G_{ij} element of $[G]$ is based on the one-loop-at-a-time approach. The loop connecting the jth output y_j to the ith input u_i of the closed-loop system is opened, and the SISO transfer function between the resulting open points is multiplied by the nominal value of G_{ij}. The resulting open-closed loop system is then subject to standard SISO stability margin analysis. Expressions for direct calculations of the gain and phase margins and their derivatives with respect to structural and control-gain variables are given in Ref. 5. In particular, the upper (lower) gain margin indicates the lowest relative increase (decrease) in the loop gain G_{ij} for which the closed-loop system becomes unstable (with all other loops closed).

The classical gain-margin analysis can also be applied for finding the stability boundaries with respect to a set of real uncertain parameters. For the sake of simplicity, the case of three such parameters is considered. Although the proposed analysis can be similarly carried out for a larger number of parameters with geometric growth in number of calculations, the main goals of presenting the stability boundaries are physical insight and design guidelines. Hypersurfaces of higher dimensions are not practical unless decomposed into families of two-dimensional curves or three-dimensional surfaces. To determine the stability boundaries, the three uncertain parameters, δ_1, δ_2, and δ_3 are interpreted as real feedback gains, and the respective gain margins are computed in a standard manner. The stability boundary in three-dimensional space can be determined by generating a grid for two of its coordinates, for example, δ_2 and δ_3, and then computing the SISO gain margin with respect to δ_1 for each grid point in the δ_2–δ_3 plane, where the uncertainty loops of δ_2 and δ_3 are closed with the respective grid-point values. The collection of all of these gain margins define the stability boundary in a three-dimensional cube of allowable $\{|\delta_i| \le 1, i = 1, 2, 3\}$ variations. The cross-over frequencies associated with the gain margins can indicate the nature of the instability (flutter) mechanism.

The modern MIMO approach for robust stability analysis is based on a the small gain theorem (see Ref. 17, pp. 271–300) that addresses the stability of a homogeneous feedback system defined by a stable transfer matrix $[M(j\omega)]$ and a feedback uncertainty matrix $[\Delta(j\omega)]$ of appropriate dimension. In its simplest form, the small gain theorem states that the feedback system is stable for any stable $[\Delta(j\omega)]$ satisfying the condition

$$\|\Delta\|_\infty < 1/\|M\|_\infty \qquad (17)$$

where $\|M\|_\infty \triangleq \sup_\omega \bar{\sigma}[M(j\omega)]$ and $\bar{\sigma}[M(j\omega)]$ is the largest singular value of $[M(j\omega)]$. This theorem establishes the necessary and sufficient conditions for robust stability of systems with unstructured uncertainties, where the complex elements of $[\Delta(j\omega)]$ are fully populated and are assumed to vary independently. However, uncertainties of systems such as the ASE plant often are structured, involving typically a number of real physical parameters such as the case of mass and inertia uncertainties discussed earlier. For such systems, the inequality (17) generally provides only sufficient conditions for robust stability and, thus, may be too conservative as a robust stability design constraint.

Robustness analysis of systems with structured uncertainty is based on the computation of the structured singular value μ, defined by[12,17]

$$\mu_\Delta[M(j\omega)] \triangleq \frac{1}{\min\{\bar{\sigma}(\Delta) : \Delta \in \boldsymbol{\Delta}, \det[I - M(j\omega)\Delta] = 0\}} \qquad (18)$$

where $\boldsymbol{\Delta}$ is the set of possible structured uncertainties. If no $\Delta \in \boldsymbol{\Delta}$ makes $I - M(j\omega)\Delta$ singular, $\mu_\Delta[M(j\omega)] = 0$. To determine the robust stability of a systems with structured uncertainties, the maximum value of μ over the entire frequency range $\omega \in [0, \infty]$ must be computed. If this maximum value is less than unity, the system is stable for all $\Delta \in \boldsymbol{\Delta}$ and $\|\Delta\|_\infty < 1$.

In most cases of structured uncertainties, there is no analytical expressions for computing μ. The available numerical algorithms

calculate upper and lower bounds of μ that are expected to converge toward each other.[9] Often, however, these bounds do not converge, especially for systems involving pure-real parametric uncertainties, as is the case in ASE systems without the model residualization uncertainty block. The upper bound of μ in such cases might be too conservative for practical design. Calculating the maximal μ involves an additional numerical search over frequency. The SISO gain-margin approach described earlier may offer a practical alternative for computing the peak μ value and the associated worst-case perturbations (uncertainties) for cases of few (up to three) uncertain parameters.

To determine the peak μ value for real uncertainties, the maximum-volume hypercube that only touches the stability boundary hypersurface at one or more points but does not intersect it must be found. The peak μ value is twice the reciprocal of the cube's vertex length. The coordinates of the common point(s) of the hypercube and the stability boundary define the worst-case perturbations, whereas the gain-margin frequency of that point on the stability hypersurface determines the frequency of the peak μ value. A simple numerical search procedure is used to construct this cube in a three-dimensional case for a sample aircraft design case presented in the following section.

Aeroservoelastic Design Example

Baseline Aeroelastic System

The numerical design example is based on the aeroelastic model of a generic advanced fighter aluminum (AFA) aircraft. The finite element ASTROS model of AFA has an all movable horizontal tail and four control surfaces on each wing. The aircraft structural model is shown in Fig. 2. The skin of the wing torsion box is subject to structural optimization. The structural design variables are the thickness of the upper and lower aluminum skins at 13 design zones of the wing torsion box, as shown in Fig. 3, leading to a total of 26 structural design variables. More details on this model can be found in Refs. 18 and 19, where the model is optimized for minimum weight, with only stress and static aeroelastic constraints.

The model used to compute the doublet-lattice unsteady aerodynamics of AFA is presented in Ref. 8. The model consists of nine aerodynamic panels representing the fuselage, inboard and outboard parts of the wing, four control surfaces, a tip missile, and a horizontal tail.

An aircraft baseline structure was created using the optimization methodology presented in Ref. 8. The baseline values of the structural design variables were obtained by an optimization process with stress and open-loop flutter constraints using the modal-based ASTROS version of Ref. 19. The flutter constraints required stability of the ASE system for 10 air velocity values of up to $V = 1105.2$ ft/s (design velocity plus 10%). For the sake of clarity and simplicity, flutter analysis was performed only with antisymmetric boundary conditions at Mach 0.9. There were 13 reduced-frequency values between 0.0 and 0.29 used to generate the aerodynamic database. The stress constraints of Ref. 8 were alleviated to obtain a design

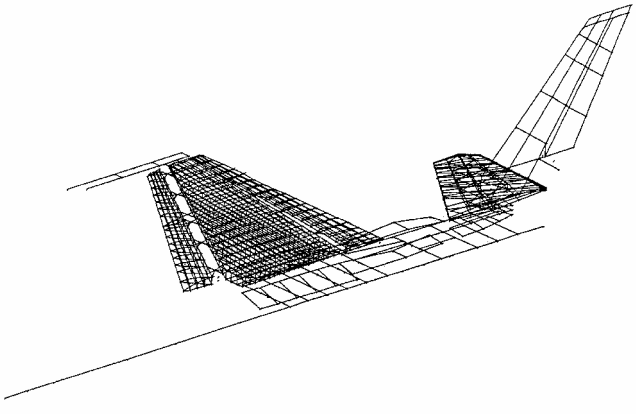

Fig. 2 AFA structural model.

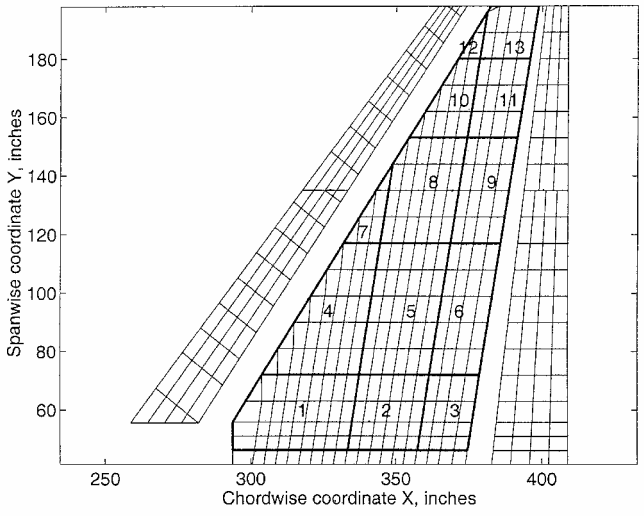

Fig. 3 AFA wing structural model with design zones.

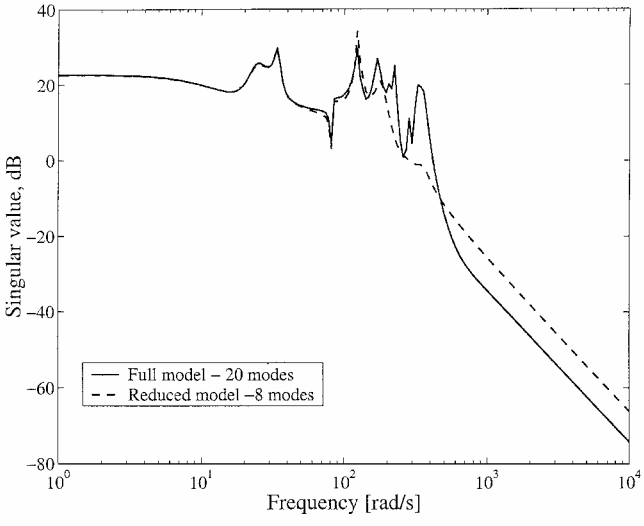

Fig. 4 Singular value plots for the full and residualized open-loop baseline ASE models.

case with a significant control–structure interaction. The resulting wing-box skin became about 30% lighter than that of Ref. 8, which reduced the wing torsional stiffness and consequently the aeroelastic effectiveness of the trailing-edge control surfaces. To compensate for the reduction in control effectiveness, all four wing control surfaces were used in the current work for roll maneuvers.

A state-space plant model for subsequent control analysis was constructed at $V = 1105.2$ ft/s with 40 structural states that represent 20 low-frequency modes including 1 rigid-body roll mode, 10 aerodynamic states, and 12 actuator states that represent the 4 wing control-surface actuators. A total of 62 states were used. The inputs to the ASE plant were the four actuators commands. The only output was the roll rate at the fuselage centerline.

To facilitate a robust design with respect to a variety of tip missiles, relatively large variations of the tip-missile inertial properties were defined as parametric uncertainties. No changes in the missile aerodynamic and elastic properties were allowed. The uncertainties of the tip missile mass and the moment of inertia about its c.g. were assumed to be $\pm 30\%$ of their nominal values, whereas the uncertainty of the tip-missile c.g. was set to ± 0.83 ft. A reduced-order baseline ASE model was obtained via static residualization of 12 structural modes (modes number 4 and 10–20). Singular value plots of the full- (20 modes, 62 states) and reduced-order (8 modes, 38 states) plant models are shown in Fig. 4, which demonstrates good approximation accuracy in the low-frequency range and significant high-frequency residualization errors.

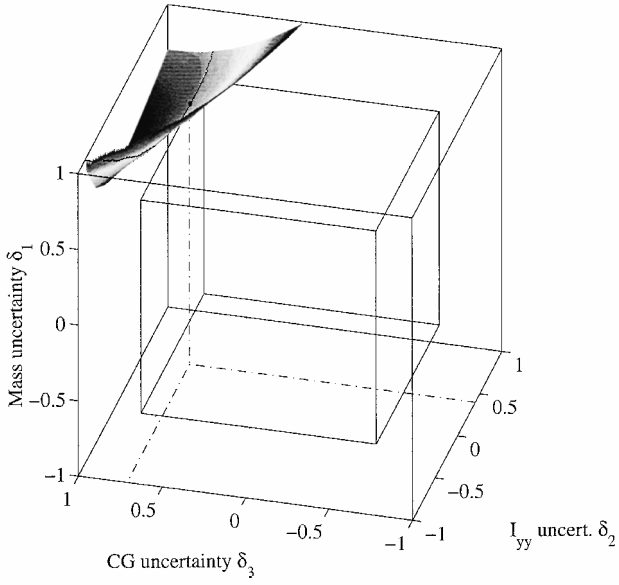

Fig. 5 Stability boundary of the open-loop baseline ASE system.

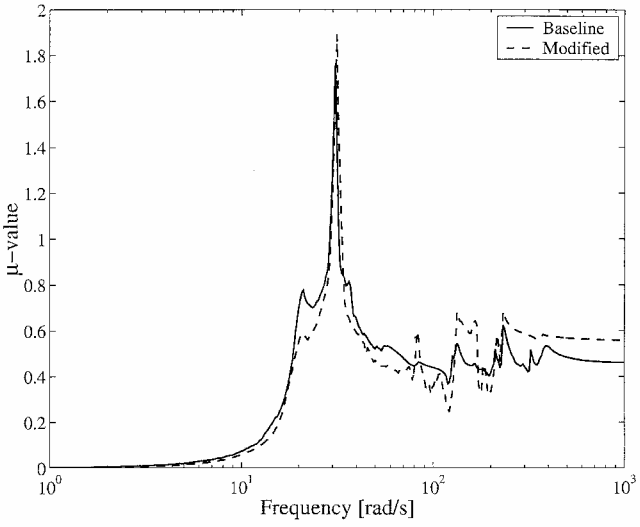

Fig. 6 Structured singular value of the open-loop ASE systems.

The open-loop stability boundary of the full-order aeroelastic model, calculated by the SISO gain-margin technique described earlier, is plotted inside the normalized uncertainty cube in Fig. 5. The region of instability of the perturbed system is above the stability boundary. A smaller cube, which has one common point with the stability boundary, is also shown. This cube, the vertex of which is 1.42 long, defines the peak real μ value as $\mu_{\text{peak}} = 2/1.42 = 1.4085$. The point of contact between the cube and the stability surface defines the flutter parameters. On the stability surface, the frequency associated with the touching point specifies the frequency where μ_{peak} occurs, that is, the flutter frequency, which in this case is $\omega_{\text{peak}} = 30.42$ rad/s. The coordinates of the touching point determine the worst-case perturbation, $[\delta_1 \ \delta_2 \ \delta_3] = [0.71 \ 0.40 \ 0.71]$, namely, 21% increase in the wing-tip missile mass, 12% increase in its pitch moment of inertia, and 0.059-ft backward shift of its c.g. The stability boundary obtained for the reduced-order model was practically identical to that of the full-order model.

The μ upper-bound plot created for the baseline model using μ tools[9] of MATLAB is shown in Fig. 6 together with that of the modified model that will be discussed later. The upper-bound μ_{peak} value is 1.7629, considerably larger than the exact value of 1.4085 computed earlier, whereas the frequencies associated with the two μ_{peak} values are similar. This implies that μ tools compute a conservative bound of the MIMO stability margin guaranteeing robust stability in a cube with a vertex length of $2/\mu_{\text{peak}} = 1.1345$, which is 20% smaller relative to the actual bound. In addition to being more accurate, the stability boundary plot of Fig. 5 clearly indicates that tip stores with higher mass and/or more rearward c.g. locations relative to those of the nominal store location cause reduction of the flutter margins. When the relatively large mass perturbations in the given example are considered, Fig. 5 provides important physical insight.

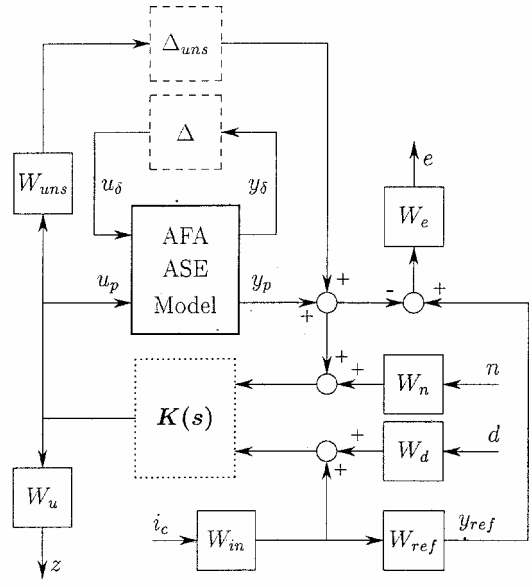

Fig. 7 Robust-control design interconnection model.

Robust Controller Design

A general interconnection model used for a robust controller design for the ASE plant is presented in Fig. 7. It incorporates the plant dynamics model of Eqs. (15) with its uncertainties, performance specification functions, and design constraints. The plant model includes the uncertainty inputs $\{u_\delta\}$ and outputs $\{y_\delta\}$. The (structured) uncertainty matrix Δ is diagonal with n_u elements $-1 \le \delta_i \le 1$ that represent the normalized physical uncertainties. When connected through Δ, the modified plant model represents the allowable perturbation of the original system around the nominal design point. The unstructured residualization uncertainty of the reduced-order model is represented by the weighting function W_{uns} and a complex scalar Δ_{uns}. The performance and design constraints are specified using the various weighting functions $W_{(\cdot)}$. The synthesis results in a dynamic controller $K(s)$.

In the current example, a lateral, robust control system is designed for the AFA example with the goal of providing category A military standard (MIL-STD) roll performance,[20] namely, roll of 90 deg in 1.4 s, 180 deg in 2.3 s, and 360 deg in 4.1 s. A detailed description of a robust controller design, with application to roll control of a fighter aircraft with uncertainties of the inertial properties of its tip missile, is given in Ref. 8. The current application defers from the former by reduced torsional stiffness of the structure and by using all four wing control surfaces for maneuvering, which leads to more challenging design specifications.

The main design goal is to provide robust aeroservoelastic stability and user-defined roll-rate performance of the aircraft. Acceptable roll performance is defined by a reference transfer function

$$W_{\text{ref}}(s) = \frac{2.076}{(0.2s+1)(0.27s+1)} \tag{19}$$

which describes a desired reference roll-rate response to the pilot roll command, and an error transfer function $W_e(s) = 5/(0.08s+1)$, which specifies the allowable deviation from the reference response. The transfer functions chosen for $W_{\text{ref}}(s)$ and $W_e(s)$ guaranty compliance with the MIL-STD requirements[20] mentioned earlier. The input function $W_{\text{in}}(s) = (0.01s+1)/(0.2s+1)$ specifies the intensity

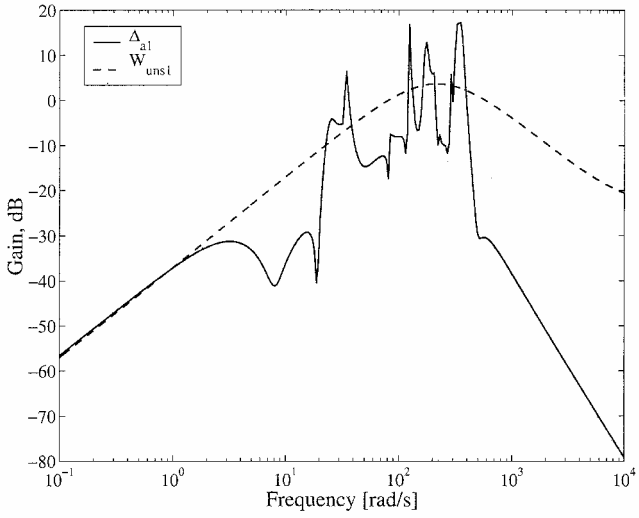

Fig. 8 Unstructured uncertainty: first input to output residualization modeling error.

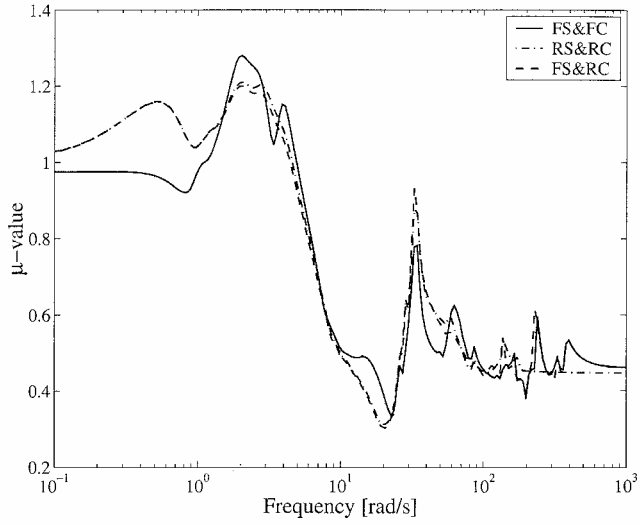

Fig. 9 Structured singular value of the closed-loop baseline ASE system.

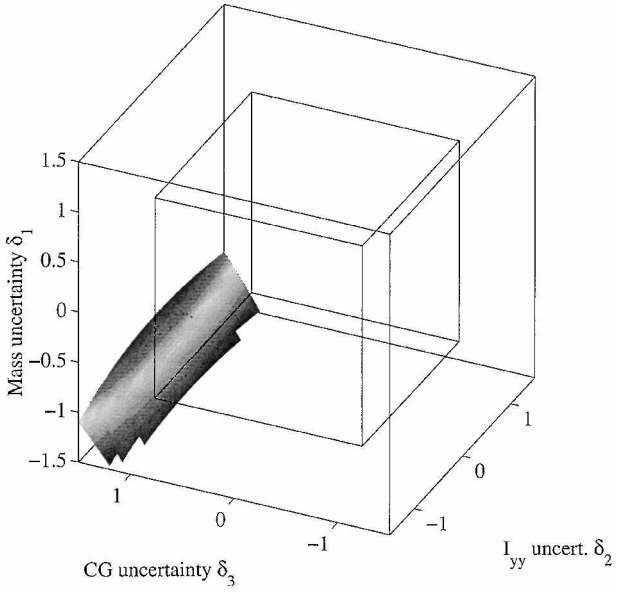

Fig. 10 Stability boundary of the closed-loop baseline ASE system.

and bandlimit of the pilot command, which is typically set to 1 Hz based on common pilot response characteristics.

The inputs to the controller are the measured pilot commands and the measured aircraft roll rate. Both signals are assumed to be contaminated with additive white measurement noise with power spectral densities specified by the constants W_d and W_n, which were set to typical values of 2×10^{-3} in appropriate units. Roll maneuvers are performed by antisymmetric deflection of the four wing control surfaces. These deflections are limited by setting the actuator weighting function W_u to the reciprocal of a realistic motion limit of 10 deg for the leading-edge ailerons and of 13 deg for the trailing-edge ailerons.

The controller designs for the full-order and for the reduced-order models were performed without the unstructured uncertainty W_{uns}. The controller obtained using the reduced-order model caused instability when applied to the full-order plant model. This implies that the residualization process entailed a significant modeling error that has to be addressed (modeled) before a controller is designed. Consequently only reduced-order models with unstructured residualization uncertainty were used for the controller design. These controllers were then evaluated on the full-order system.

To account for the residualization errors, an additive unstructured uncertainty was defined as

$$\Delta_a(j\omega) = G(j\omega) - G_r(j\omega) \tag{20}$$

where $G(j\omega)$ and $G_r(j\omega)$ are the transfer matrices of the full- and reduced-order models, respectively. The unstructured uncertainty $\Delta_a(j\omega)$ has four inputs (the actuator commands) and one output (the measured roll-rate signal). Frequency-response magnitudes for all channels were approximated by second-order rational transfer functions $W_{\text{uns}_i}(s), i = 1, \ldots, 4$. The residualization error was constructed based on these transfer functions $W_{\text{uns}} = [W_{\text{uns}_1}\ W_{\text{uns}_2}\ W_{\text{uns}_3}\ W_{\text{uns}_4}]$. Minimal realization of this 1×4 transfer matrix led to a third-order unstructured uncertainty model. As an example, exact and approximated unstructured uncertainty plots for the first channel, from outboard trailing-edge actuator to the roll-rate sensor, are shown in Fig. 8. This approximation was found to be sufficient to capture the residualization effects, although a more conservative overbounding approximation could have been used, too, with a slight compromise in the closed-loop performance.

A robust controller was designed for the reduced-order system (RS) with the parametric and unstructured uncertainties using the μ synthesis technique. The design converged after 5 D-K iterations, leading to a 157th-order controller. The order of this controller was reduced to 42 using the balanced truncation method with a minimal effect on the structured singular value μ. The controller designed using the RS model and then order reduced as detailed earlier will be called in the sequel the reduced controller (RC). For comparison, a robust μ controller was designed for the full-order system (FS) with parametric uncertainties only. The design converged after 5 D-K iterations to a 168-order controller that was order reduced to 56 with a negligible effect on the value of μ. The controller designed using the full-order model and then order reduced will be referred to as the full controller (FC). Even though the resulting controller orders for the full- and reduced-order designs are similar, the computational time for the reduced design is considerably shorter because of lower plant order.

Figure 9 presents the structured singular values μ of three controller–system combinations: FS with FC, RS with RC, and FS with RC. The controller designed using the reduced-order model with unstructured uncertainty (RC) exhibits very similar performance when evaluated with the full- and reduced-order models, demonstrated by the close dashed line and dashed-dotted line in Fig. 9. In addition, the reduced-order controller provides higher robustness than the full-order controller, expressed by the 6% lower μ peak value obtained using the former.

The structured singular value plots of Fig. 9 present a violation of the requirement for $\mu_{\text{peak}} \leq 1$, indicating that the robust performance specifications were not met with either of the two controllers. The low frequency at which μ_{peak} is attained suggest that the robust performance, rather than robust stability, is violated. This is verified by examining the closed-loop stability boundary of Fig. 10

that was calculated for the closed-loop system with the reduced-order controller. It shows the uncertainty cube inside the stability boundary. Thus, this μ controller suppresses flutter in the specified range of uncertainties, however, does not provide the required roll performance.

Multidisciplinary Design Optimization

A multidisciplinary optimization (MDO) procedure was applied next to meet the required performance specifications. The robust controller was connected to the full ASE model through four additional controller input design gains, the nominal values of which are one. The resulting closed-loop model was then subject to mixed structural and control optimization using a modified version of ASTROS.[6] The flutter constrains were identical to those used to derive the baseline structure. Proper control-related constraints were defined after several optimization and controller design attempts. As a result, constraints for a total dc gain of the open-loop system from the trailing-edge control surfaces to the sensor (control effectiveness) were increased by 20% compared to the baseline structure. In addition, constraints on the minimum singular values of the closed-loop system were set to 90% of the baseline structure, that is, a 10% reduction. The four controller input gains were also used in the optimization. Clearly, this results only in suboptimal controller designs due to the fixed values of most of its parameters. However, it was found that it improves the overall MDO process due to the added flexibility.

The optimization led to a reduced structural weight of 312.2 lb, which is smaller than the baseline weight of 321.8 lb and distributed differently. The modified open-loop structure exhibits reduced robustness to a structured uncertainty compared to the heavier baseline structure, as shown in Fig. 11. Here, $\mu_{\text{peak}} = 1.5625$ at frequency $\omega_{\text{peak}} = 31.39$ rad/s, and the worst-case perturbation is $[\delta_1 \ \delta_2 \ \delta_3] = [0.64 \ -0.20 \ 0.64]$, corresponding to 19% increase in the missile mass, 6% decrease in its pitch moment of inertia, and 0.53-ft backward c.g. shift. As for the baseline, the upper-bound μ_{peak} calculated using MATLAB (Fig. 6) is 1.8884, considerably larger than the exact value.

Controller design based on the reduced-order model was performed for the modified structure, while using the same eight modes as in the baseline case. A new approximated unstructured uncertainty W_{uns} was constructed for the new structure. Its shape and parameters were similar to the baseline case. The design process converged after 4 D-K iterations, with a structured singular of $\mu_{\text{peak}} = 1.008$. The 45th-order controller was order reduced using the balanced truncation technique to 33 with a negligible effect on the value of μ. For comparison, control design for the full modified

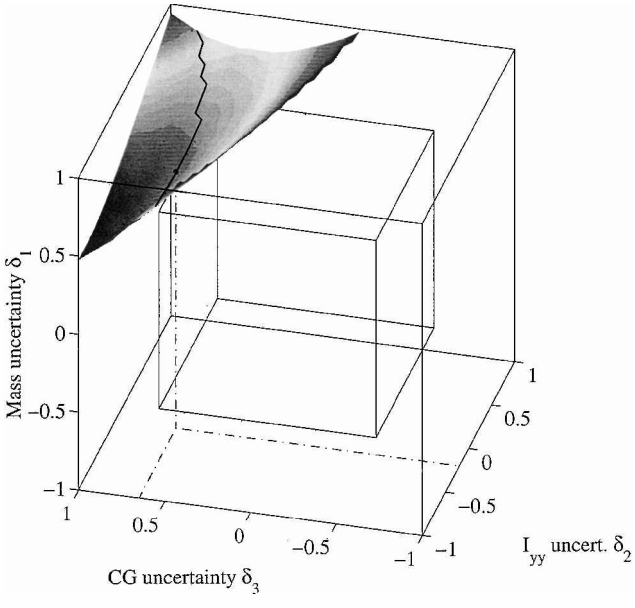

Fig. 11 Stability boundary of the open-loop modified ASE system.

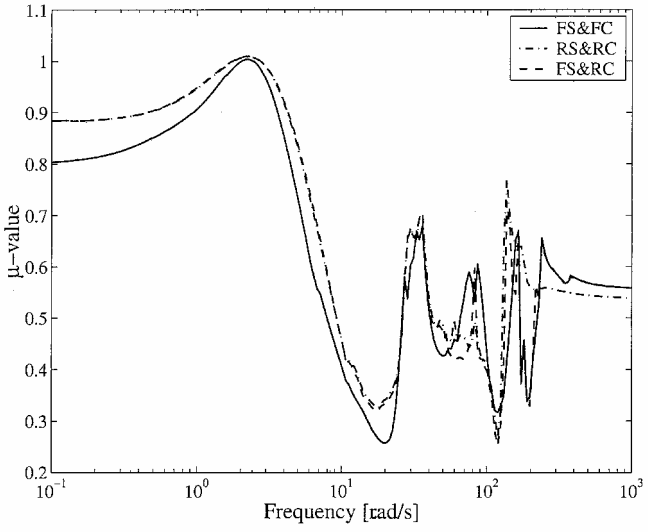

Fig. 12 Structured singular values for the closed-loop modified ASE system.

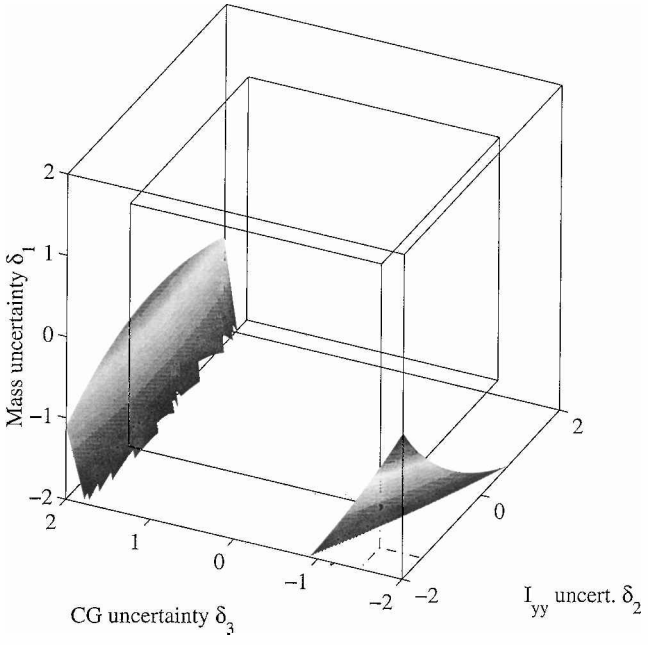

Fig. 13 Stability boundary of the closed-loop modified ASE system.

model converged after 6 D-K iterations with $\mu_{\text{peak}} = 1.004$ and a 98th-order controller that was order reduced to 45.

The structured singular value plots for the full model and reduced model (with unstructured uncertainty) designs are shown in Fig. 12. The controller RC designed using the reduced-order model and evaluated with the FS exhibits good performance, similar to that of a controller FC designed using the FS. This clearly justifies the use of reduced order modeling for efficient ASE design and multidisciplinary optimization. The robust stability boundary of the closed-loop system with the reduced-order controller is shown in Fig. 13 which demonstrates that the robust stability requirements, while neglecting the performance specifications, are met in a larger cube than for the closed-loop baseline case of Fig. 10. Here $\mu_{\text{peak}} = 0.6689$, which implies an uncertainty cube with a vertex of a length 2.99. The worst-case perturbations are defined by the corner of the cube that touches the stability boundary that leads to the equal perturbation values $[\delta_1 \ \delta_2 \ \delta_3] = [-1.495 \ -1.495 \ -1.495]$, namely, 45% decrease in the wing-tip missile mass and in its pitch moment of inertia and 1.25-ft forward shift of its c.g. These robust stability bounds clearly exceed the uncertainty specifications, however, are needed to guarantee robust performance.

Conclusions

A methodology for robust design of MIMO uncertain aeroservoelastic systems is integrated with structural and control synthesis methods. The resulting design tools facilitate efficient MDO processes that incorporate modern methods of robust-control analysis and synthesis. A methodology for reduced-order modeling of uncertain or perturbed ASE systems is developed. The use of structured uncertainties to represent perturbations and variations in the reduced-order ASE model minimizes the uncertainty overbounding, whereas unstructured uncertainties allow the elimination of the undesirable effects of frequency-dependent model reduction errors on the robust controller design. The use of the robust-control design techniques within a multidisciplinary design scenario is demonstrated in cases of simultaneous aircraft performance and flutter suppression requirements. An application of the classical gain-margin formulation with modern uncertainty modeling facilitates a new procedure for mapping flutter (instability) boundaries in a three-dimensional uncertainty space. These boundaries can be instrumental in practical design cases. They also provide the means for a practical and accurate evaluation of the peak structured singular values in cases of real parameter uncertainties, where modern μ-analysis tools might fail. The new procedures advance the integration of structural dynamics, unsteady aerodynamics, and control systems into unified formulation and software design tools.

References

[1]Livne, E., "Integrated Aeroservoelastic Optimization: Status and Direction," *Journal of Aircraft*, Vol. 36, No. 1, 1999, pp. 122–145.

[2]Karpel, M., "Reduced-Order Models for Integrated Aeroservoelastic Optimization," *Journal of Aircraft*, Vol. 36, No. 1, 1999, pp. 146–155.

[3]Karpel, M., "Time-Domain Aeroservoelastic Modeling Using Weighted Unsteady Aerodynamic Forces," *Journal of Guidance, Control, and Dynamics*, Vol. 13, No. 1, 1990, pp. 30–37.

[4]Karpel, M., and Strul, E., "Minimum-State Unsteady Aerodynamic Approximations with Flexible Constraints," *Journal of Aircraft*, Vol. 33, No. 6, 1996, pp. 1190–1196.

[5]Idan, M., Karpel, M., and Moulin, B., "Aeroservoelastic Interaction Between Aircraft Structural and Control Design Schemes," *Journal of Guidance, Control, and Dynamics*, Vol. 22, No. 4, 1999, pp. 513–519.

[6]Chen, P. C., Liu, D., Sarhaddi, D., Striz, A. G., Neill, D. J., and Karpel, M., "Enhancement of the Aeroservoelastic Capability in ASTROS," U.S. Air Force Research Lab., WL-TR-96-3119, Wright–Patterson AFB, OH, Sept. 1996.

[7]"ZAERO—Theoretical Manual," Ver. 4.2, ZONA Technology, Scottsdale, AZ, May 2000.

[8]Moulin, B., Idan, M., and Karpel, M., "Aeroservoelastic Structural and Control Optimization Using Robust Design Schemes," *Journal of Guidance, Control, and Dynamics*, Vol. 25, No. 1, 2002, pp. 152–159.

[9]Balas, G. J., Doyle, J. C., Glover, K., Packard, A., and Smith, R., "μ-Analysis and Synthesis Toolbox for Use with MATLAB. User's Guide. Version 3," MathWorks Natick, MA, 1998.

[10]Lind, R., and Brenner, M., *Robust Aeroservoelastic Stability Analysis*, Advances in Industrial Control, Springer, London, 1999, pp. 470–477.

[11]Karpel, M., "Size-Reduction Techniques for the Determination of Efficient Aeroservoelastic Models," *Control and Dynamic Systems*, Academic Press, San Diego, CA, Vol. 54, 1992, pp. 263–295.

[12]Doyle, J. C., Packard, A., and Zhou, K., "Review of LFTs, LMIs and μ," *Proceedings of the IEEE Conference on Decision and Control*, Vol. 2, IEEE Press, Piscataway, NJ, 1991, pp. 1227–1232.

[13]Cockburn, J. C., and Morton, B. G., "Linear Fractional Representation of Uncertain Systems," *Automatica*, Vol. 33, No. 7, 1997, pp. 1263–1271.

[14]Belcastro, C. M., "Parametric Uncertainty Modeling: An Overview," *Proceedings of the American Control Conference*, Vol. 2, IEEE Press, Piscataway, NJ, 1998, pp. 992–996.

[15]Moulin, B., Idan, M., and Karpel, M., "Robust Control Design for Uncertain Aeroservoelastic Systems Using Reduced Order Models," AIAA Paper 2001-1583, April 2001.

[16]Ljung, L., *System Identification: Theory for the User*, 2nd Ed., Prentice–Hall, Upper Saddle River, NJ, 1999, pp. 227–233.

[17]Zhou, K., Doyle, J. C., and Glover, K., *Robust and Optimal Control*, Prentice–Hall, Upper Saddle River, NJ, 1996, pp. 271–300.

[18]Karpel, M., "Modal-Based Enhancement of Integrated Structural Design Optimization Schemes," *Journal of Aircraft*, Vol. 35, No. 3, 1998, pp. 437–444.

[19]Karpel, M., Moulin, B., and Love, M. H., "Structural Optimization with Stress and Aeroelastic Constraints Using Expandable Modal Basis," *AIAA Journal*, Vol. 36, No. 11, 1999, pp. 1514–1519.

[20]"Military Standard. Flying Qualities of Piloted Aircraft," U.S. Air Force MIL-STD-1797A, 30 Jan. 1990, pp. 436–437.